2014

The Marburg virus VP24 protein interacts with Keap1 to activate the cytoprotective antioxidant response pathway

Megan R. Edwards
Icahn School of Medicine

Britney Johnson
Washington University School of Medicine in St. Louis

Chad E. Mire
University of Texas Medical Branch

Wei Xu
Washington University School of Medicine in St. Louis

Reed S. Shabman
Icahn School of Medicine

See next page for additional authors

Cell Reports
Report

The Marburg Virus VP24 Protein Interacts with Keap1 to Activate the Cytoprotective Antioxidant Response Pathway

Megan R. Edwards,[1] Britney Johnson,[2] Chad E. Mire,[3] Wei Xu,[2] Reed S. Shabman,[1,4] Lauren N. Speller,[2] Daisy W. Leung,[2] Thomas W. Geisbert,[3] Gaya K. Amarasinghe,[2] and Christopher F. Basler[1,*]
[1]Department Microbiology, Icahn School of Medicine, Mount Sinai, New York, NY 10029, USA
[2]Department of Pathology and Immunology, Washington University School of Medicine, St. Louis, MO 63110, USA
[3]Galveston National Laboratory, Department of Microbiology and Immunology, University of Texas Medical Branch, Galveston, TX 77555, USA
[4]Present address: J. Craig Venter Institute, Rockville, MD 20850, USA
*Correspondence: chris.basler@mssm.edu
http://dx.doi.org/10.1016/j.celrep.2014.01.043

SUMMARY

Kelch-like ECH-associated protein 1 (Keap1) is a ubiquitin E3 ligase specificity factor that targets transcription factor nuclear factor (erythroid-derived 2)-like 2 (Nrf2) for ubiquitination and degradation. Disrupting Keap1-Nrf2 interaction stabilizes Nrf2, resulting in Nrf2 nuclear accumulation, binding to antioxidant response elements (AREs), and transcription of cytoprotective genes. Marburg virus (MARV) is a zoonotic pathogen that likely uses bats as reservoir hosts. We demonstrate that MARV protein VP24 (mVP24) binds the Kelch domain of either human or bat Keap1. This binding is of high affinity and 1:1 stoichiometry and activates Nrf2. Modeling based on the Zaire ebolavirus (EBOV) VP24 (eVP24) structure identified in mVP24 an acidic loop (K-loop) critical for Keap1 interaction. Transfer of the K-loop to eVP24, which otherwise does not bind Keap1, confers Keap1 binding and Nrf2 activation, and infection by MARV, but not EBOV, activates ARE gene expression. Therefore, MARV targets Keap1 to activate Nrf2-induced cytoprotective responses during infection.

INTRODUCTION

Kelch-like ECH-associated protein 1 (Keap1) is a cellular adaptor protein that links the Cul3/Rbx1 (Roc1) ubiquitin E3 ligase to the oxidative stress response through its interaction with the transcription factor nuclear factor (erythroid-derived 2)-like 2 (Nrf2) (reviewed in Copple, 2012). Under homeostatic conditions, Keap1 suppresses the cellular antioxidant transcriptional program by directing the ubiquitin-mediated degradation of Nrf2 (Itoh et al., 1999; McMahon et al., 2003). Keap1 interacts, via its Kelch domain, with two sites located in the Nrf2-ECH homology-2 (Neh2) domain of Nrf2 (Itoh et al., 1999; Tong et al., 2006). Disruption of Nrf2-Keap1 interaction leads to transcription of genes possessing antioxidant response elements (AREs) (Tong et al., 2007). The upregulated ARE genes encode proteins involved in detoxification reactions, cell survival, and immune modulation (reviewed in Baird and Dinkova-Kostova, 2011; Ma, 2013).

ARE responses impact the outcome of viral infections. For example, the Nrf2 pathway inhibits influenza virus and respiratory syncytial virus replication in cell culture and in vivo (Cho et al., 2009; Kesic et al., 2011). In contrast, for hepatitis B virus, hepatitis C virus, and human cytomegalovirus, induction of ARE responses may protect infected cells from oxidative damage and influence immune responses by modulating immunoproteasome function (Burdette et al., 2010; Ivanov et al., 2011; Lee et al., 2013; Schaedler et al., 2010).

Marburg viruses (MARVs) and Ebola viruses (EBOVs), members of the family *Filoviridae*, are emerging, zoonotic pathogens that likely use bats as reservoir hosts. Filoviruses are of concern because they cause hemorrhagic fever with a high fatality rate in humans (reviewed in Brauburger et al., 2012). Filoviruses encode multifunctional VP24 proteins, which play important roles in the formation of viral nucleocapsids, release of infectious virus particles, and modulation of viral RNA synthesis (Bamberg et al., 2005; Beniac et al., 2012; Bharat et al., 2011, 2012; Hoenen et al., 2006; Huang et al., 2002; Mateo et al., 2011; Noda et al., 2006; Watanabe et al., 2007; Wenigenrath et al., 2010). In addition, EBOV VP24 (eVP24) disrupts interferon (IFN) signaling pathways and interacts with select karyopherin α proteins (KPNAs), thereby blocking nuclear accumulation of tyrosine-phosphorylated STAT1 (Mateo et al., 2010; Reid et al., 2006, 2007). In contrast, MARV VP24 (mVP24) neither interacts with KPNAs nor inhibits IFN signaling, and functionally relevant interactions with host factors have not previously been defined (Valmas et al., 2010). However, a recent mass spectrometry screen identified Keap1 as a potential mVP24 binding partner (Pichlmair et al., 2012).

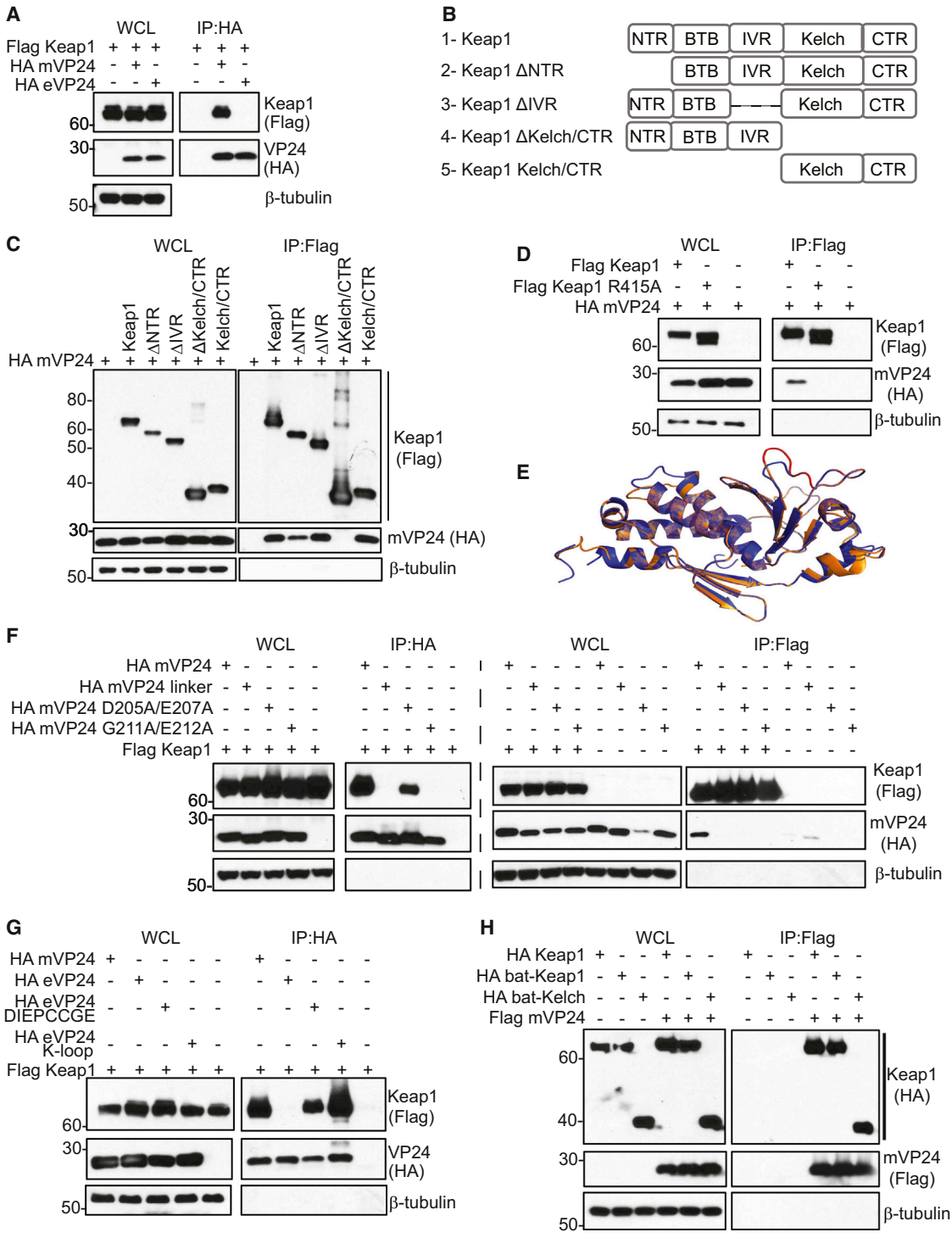

Figure 1. mVP24 Interacts with Keap1 in CoIP Assays

(A) coIPs with HA antibody were performed on lysates of HEK293T cells cotransfected with plasmids for Flag-Keap1 and HA-mVP24 or HA-eVP24. Western blots were performed for Flag and HA. WCL, whole cell lysate; IP, immunoprecipitation.

(B) Schematic diagram of Flag-tagged Keap1 domain deletion mutants used in (C).

(C) Flag-Keap1 domain deletion mutant constructs were coexpressed in HEK293T cells with HA-mVP24 and analyzed by coIP with Flag antibody.

(D) HA-mVP24 and either Flag-Keap1 or Flag-Keap1 R415A were analyzed by coIP as in (C).

(E) Overlay of the mVP24 structural model (orange) on the determined eVP24 structure (purple). The mVP24 K-loop (amino acids 205–212) is indicated in red.

(legend continued on next page)

To date, the described mechanisms by which viruses engage the ARE response do not involve direct interaction with components of the signaling pathways. Rather, viruses are demonstrated to activate other signaling pathways or induce oxidative stress, indirectly activating antioxidant responses. Here, we demonstrate that mVP24 but not eVP24 directly interacts with the human and bat Keap1 proteins. We further define the basis of the interaction and demonstrate that expression of mVP24 but not eVP24 activates Nrf2, triggering cytoprotective responses. Correspondingly, MARV but not EBOV infection activates ARE gene expression. Collectively, these data suggest that MARV evolved to specifically target a host cytoprotective gene expression program to facilitate its replication.

RESULTS

mVP24 Interacts with Keap1

Coimmunoprecipitation (coIP) assays demonstrated that Flag-tagged Keap1 interacts with HA-mVP24, but not with HA-eVP24 (Figure 1A). Keap1 contains several previously defined domains: the N-terminal region (NTR); the Bric-a-Brac, Tramtrack, Broad complex (BTB) domain; the intervening region (IVR); and the Kelch domain/C-terminal region (CTR) (Komatsu et al., 2010). Domain deletion mutants of Keap1 and a construct comprising only the Kelch domain/CTR were tested for mVP24 interaction by coIP (Figure 1B). The NTR and IVR deletion mutants retained interaction, whereas deletion of the Kelch/CTR resulted in loss of interaction (Figure 1C). The isolated Kelch/CTR domain also interacted with mVP24 (Figure 1C). Therefore, the Kelch/CTR domain is necessary and sufficient to interact with mVP24 (Figure 1C). The mutation to alanine of Keap1 Kelch domain residue R415 disrupts interaction with Nrf2 (Lo et al., 2006). Similarly, Keap1 R415A did not coprecipitate with mVP24 (Figure 1D), suggesting that Nrf2 and mVP24 interact with the Keap1 Kelch region in a similar fashion.

To gain insight into the region(s) of mVP24 required to interact with Keap1, we used our recently solved structure of VP24 from Zaire EBOV, which is very similar to the structures of Sudan and Reston eVP24s (Zhang et al., 2012) (see Supplemental Experimental Procedures, Supplemental Results, and Table S1), and the Phyre2 software package to obtain a molecular model of mVP24 (Kelley and Sternberg, 2009). The resulting structural model identified a loop (the K-loop, amino acids 202–212) that is likely solvent exposed (Figure 1E). The sequence near the K-loop is not well conserved among filoviral VP24 proteins. This loop contains a sequence DIEPCCGE that is reminiscent of the high-affinity binding motif of DXXTGE, used by Nrf2 to interact with the Keap1 Kelch domain (Lo et al., 2006). Among the several Keap1 Kelch domain binding determinants, "GE" motifs appear to be the most highly conserved, with nearby upstream acidic residues also playing an important role for several interacting partners (Komatsu et al., 2010; Padmanabhan et al., 2008). Given this similarity, we made three HA-tagged mVP24 constructs (Figure 1F). In "mVP24 linker," the 205-DIEPCCGE-212 sequence was replaced with a serine-glycine linker. "mVP24 D205A/E207A" and "mVP24 G211A/E212A" were designed based on analogous loss-of-binding mutants described for cellular Keap1-interactor p62 (Komatsu et al., 2010). By coIP, wild-type mVP24 strongly interacted with Keap1, mVP24 D205A/E207A interacted weakly, and no interaction was detected with either mVP24 linker or mVP24 G211A/E212A (Figure 1F). To assess the role of the DIEPCCGE motif for interaction with Keap1, DIEPCCGE was swapped in place of the corresponding residues within eVP24, creating "eVP24 DIEPCCGE." We also replaced the loop of eVP24 (202-QEPDKSAMDIRHPGPV-217) with the mVP24 K-loop (202-RRIDIEPCCGETVLSESV-219), creating the "eVP24 K-loop." eVP24 DIEPCCGE and eVP24 K-loop interacted with Keap1, with the full K-loop appearing to confer better binding, whereas wild-type eVP24 once again did not interact with Keap1 (Figure 1G). These results demonstrate that the DIEPCCGE sequence and the K-loop, when placed in the context of the VP24 structural scaffold, play a critical role for mVP24-Keap1 interaction.

MARVs likely use bats as reservoir hosts (Amman et al., 2012; Towner et al., 2009). Therefore, a specific viral interaction with Keap1 likely evolved and should be conserved in bats. Alignment of human Keap1 and two divergent bat species, a microbat (*Myotis lucifugus*) and a megabat (*Pteropus alecto*), revealed 97% amino acid identity between human and microbat Keap1 and 98% amino acid identity between human and megabat Keap1 (data not shown). Full-length Keap1 (bat-Keap1) and Kelch domain (bat-Kelch) constructs were generated from an available microbat (*Myotis velifer incautus*) cell line. Both coprecipitate with mVP24 with efficiencies similar to that of human Keap1 (Figure 1H).

Keap1 inhibits ARE gene expression through its interaction with Nrf2 (McMahon et al., 2003). When Keap1 repression is relieved, which can be due to posttranslational modification of Keap1 or interaction with select Kelch domain binding partners such as p62, Nrf2 translocates to the nucleus and activates ARE gene expression (Itoh et al., 1999; McMahon et al., 2003). To determine whether the interaction of mVP24 with the Keap1 Kelch domain activates Nrf2, a GFP-Nrf2 fusion protein was expressed alone or in the presence of Flag-Keap1 and HA-tagged wild-type mVP24, mutant mVP24 or wild-type, or chimeric eVP24s. Overexpression of Nrf2, which is known to overwhelm the available endogenous Keap1, resulted in nuclear localization of GFP-Nrf2, as expected (Figure S1). Coexpression of Keap1 retained most of the Nrf2 in the cytoplasm. Additional expression of mVP24 and eVP24-K-loop restored Nrf2-GFP nuclear localization, whereas mVP24 mutants and eVP24-DIEPCCGE, which do not interact efficiently with Keap1, did not (Figure S1; see Supplemental Results for details).

(F) Flag-Keap1 and HA-mVP24 wild-type or mutants were analyzed by coIP as in (A) and (C).
(G) Flag-Keap1 and HA-mVP24, eVP24, eVP24 DIEPCCGE, or eVP24 K-loop were coexpressed in HEK293T cells and analyzed by coIP as in (A).
(H) Flag-mVP24 and HA-Keap1, bat-Keap1, and bat-Kelch were coexpressed in HEK293T cells and analyzed by coIP as in (C).
See also Figure S1.

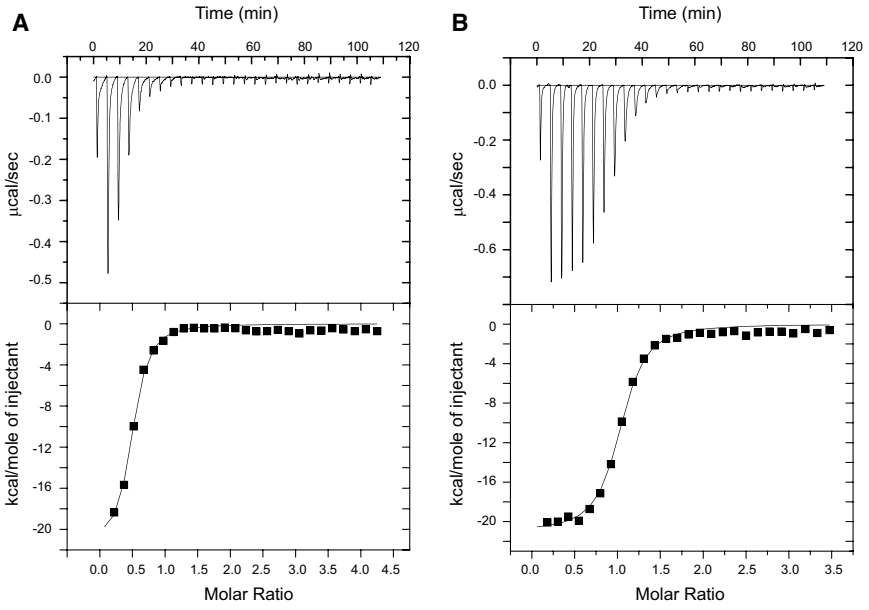

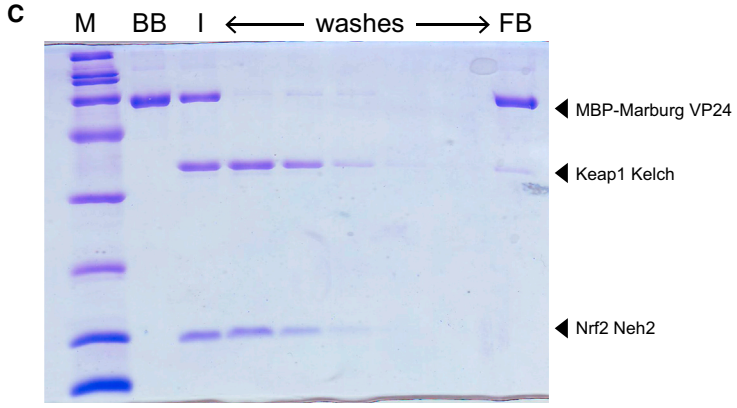

Figure 2. mVP24 Binds to Keap1 Kelch Domain with High Affinity and Specificity

(A and B) Representative ITC data for Kelch domain of Keap1 binding to (A) Nrf2 Neh2 domain and (B) mVP24. Raw heats of reaction versus time (top panels) and the integrated heats of reaction versus molar ratio of ligand to receptor (bottom panels) are shown. Thermodynamic binding parameters of $K_D = 170 \pm 60$ nM, $\Delta H = -1.96 \pm 0.1 \times 10^4$ kcal/mol, $T\Delta S = -10.4$ kcal/mol, and n (no. of sites) = 0.49 ± 0.02 for (A) and $K_D = 158 \pm 20$ nM, $\Delta H = -2.10 \pm 0.03 \times 10^4$ kcal/mol, $T\Delta S = -11.7$ kcal/mol, and n (no. of sites) = 1.00 ± 0.01 for (B) were obtained.

(C) mVP24 binding to Kelch prevents Nrf2-Neh2 interaction. Coomassie blue-stained SDS-PAGE of a pull-down assay where MBP-mVP24 was immobilized on amylose resin (BB, bound beads) is shown. Keap1 Kelch and Nrf2 Neh2 domain were subsequently added to the resin (I, input), and the resin was washed with buffer (washes). The final bound bead sample (FB, final beads) is indicated. M, molecular weight marker.

See also Figure S2.

mVP24 Binds the Keap1 Kelch Domain with High Affinity and Specificity

Binding of mVP24 to Keap1 Kelch was further evaluated by isothermal titration calorimetry (ITC), which measures heat generated by these exothermic interactions. ITC results confirmed that Keap1 Kelch binds the Nrf2 Neh2 domain with high affinity (K_D = 170 ± 60 nM) and stoichiometry (n = 0.46) (Figure 2A) and support a stoichiometry of 2:1 for Kelch binding to Neh2 with thermodynamic parameters similar to those previously reported by Tong et al. (2006). Assays under similar conditions for Kelch-mVP24 resulted in a K_D of 158 ± 20 nM (Figure 2B) with a binding stoichiometry of 1:1.

To gain additional mechanistic insight, we performed competition pull-down experiments using wild-type mVP24, eVP24, and eVP24 K-loop, which were designed based on the mVP24 structural model (Figures S2A–S2C). We established the basal binding conditions for the Kelch and Neh2 interaction by pull-down (Figure S2D) as well as Kelch binding to mVP24 (Figure S2E) and examined the ability of recombinant eVP24 (Figure S2F) and eVP24 K-loop (Figure S2G) to bind the Keap1 Kelch domain. Next, we assessed whether mVP24 can outcompete Neh2 binding to the Kelch domain. A complex between the Kelch domain and Neh2 was preformed, and the ability of an immobilized mVP24 protein to displace Neh2 from the Kelch/Neh2 complex was assessed. Despite similar affinities of Neh2 and mVP24 for Kelch domain, mVP24 can bind the Kelch domain in the presence of a 2-fold excess of Neh2 (Figure 2C). Therefore, in the absence of other factors, mVP24 displaces Nrf2 from Keap1. This provides a biochemical explanation as to how the mVP24-Keap1 interaction triggers Nrf2 nuclear localization.

mVP24 Expression Activates ARE-Directed Gene Expression

Stimuli that disrupt the Nrf2-Keap1 interaction and promote Nrf2 nuclear localization activate expression of ARE genes (reviewed in Magesh et al., 2012). We therefore assessed the ability of wild-type or mutant mVP24s to activate an ARE luciferase reporter gene. Cellular Keap1-interacting protein p62, a previously described activator of Nrf2, served as a positive control (Komatsu et al., 2010; Lau et al., 2010). Expression of mVP24 induced the ARE reporter to similar levels as p62 (Figure 3A). In contrast, mVP24 linker mutant and mVP24 G211A/E212A did not activate the ARE promoter. mVP24 D205A/E207A did activate the ARE promoter but to a lesser extent than wild-type mVP24, reflecting the residual binding activity of this mutant for Keap1 (Figure 3A). Therefore, Nrf2 activation correlates with Keap1-mVP24 binding activity (Figure 1F). In a separate experiment, expression of Nrf2 alone resulted in

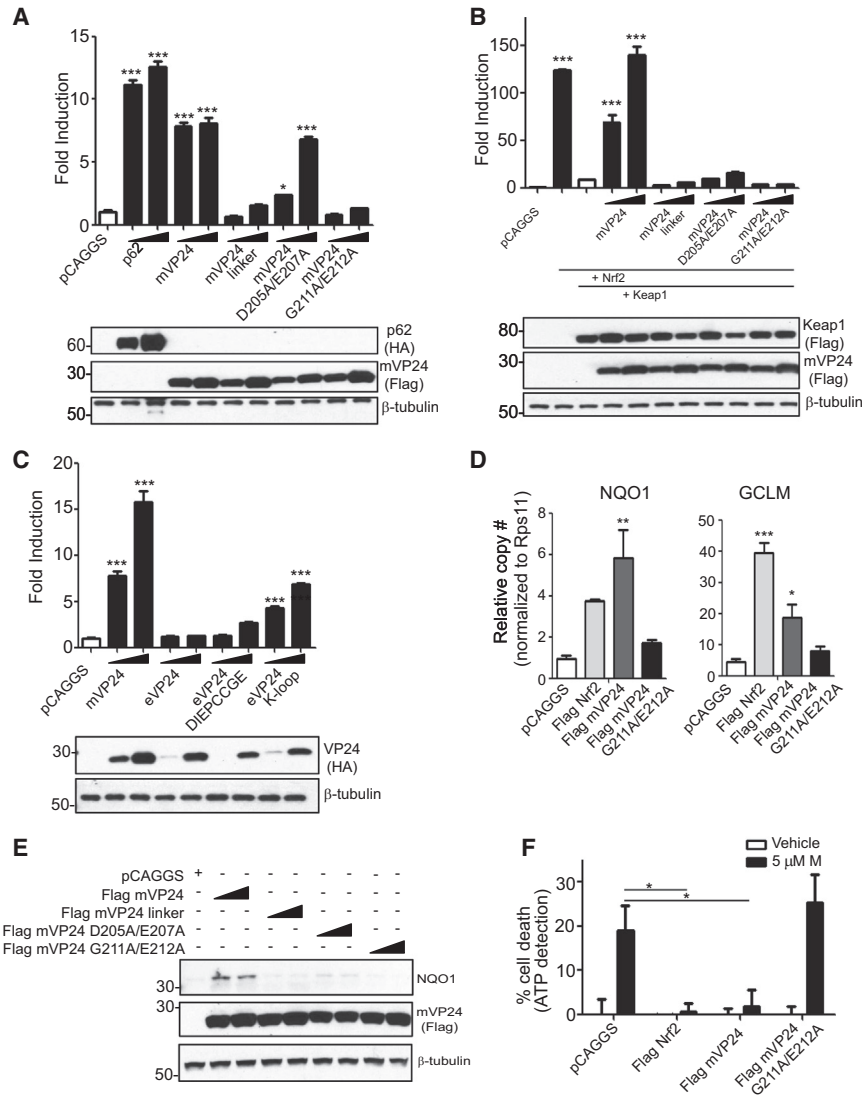

Figure 3. mVP24 Activates Expression of ARE Genes

(A and B) HEK293T cells were transfected with the ARE luciferase reporter plasmid, a constitutively expressed *Renilla* luciferase plasmid, and pCAGGS (empty vector) or increasing concentrations of HA-p62, Flag-wild-type mVP24, or mVP24 mutants. (B) Same as (A), with the additional overexpression of Flag-Nrf2 and Flag-Keap1. At 18 hr posttransfection (hpt), luciferase activity was assayed for (A) and (B). Western blots performed for HA and Flag are indicated.

(C) Same assay protocol as (A) but transfected with HA-mVP24, eVP24, or eVP24 mutants.

(D) pCAGGS, Flag-Nrf2, mVP24, or mVP24 G211A/E212A was transfected in triplicate in HEK293T cells. At 24 hpt, qRT-PCR was performed to quantify mRNAs for the indicated genes, normalized to the *RPS11* mRNA.

(E) HEK293T cells were transfected with the indicated plasmids, and 18 hpt, endogenous NQO1 was measured by western blot.

(F) Cell viability assay. HEK293T cells were transfected with pCAGGS, Flag-Nrf2, mVP24, or mVP24 G211A/E212A and 24 hpt were treated with vehicle control (ethanol) or 5 μM menadione (M) for 3 hr.

In (A)–(D), values represent the mean and SEM of triplicate samples, and statistical significance was assessed by a one-way ANOVA comparing columns to the control (white bar): ***$p < 0.001$, **$p < 0.01$, and *$p < 0.05$. Samples in (F) represent the mean and SEM of six samples, and significance was assessed by a one-way ANOVA: *$p < 0.05$.

See also Figure S3.

greater than 100-fold ARE reporter activation (Figure 3B). Keap1 coexpression inhibited the activation. mVP24 expression relieved the repression of Nrf2, resulting in ARE gene expression (Figure 3B). None of the mutant mVP24s induced significant ARE activation, despite expression comparable to that of wild-type mVP24 (Figure 3B). This suggests that the residual binding of mVP24 D205A/E207A is not sufficient to disrupt the repressive activity of the overexpressed Keap1 (Figure 3B). Although expression of eVP24 did not activate the ARE reporter, expression of the mutant eVP24-DIEPCCGE resulted in a slight increase in reporter activity, and eVP24 K-loop significantly induced ARE reporter expression (Figure 3C). Similarly, bat-Keap1 inhibited the activation of the ARE reporter by overexpressed human Nrf2 (Figure S3A), and mVP24 expression relieved the repression mediated by bat-Keap1 on the ARE reporter (Figure S3A). Therefore, mVP24 interaction with Keap1 has functional consequences because it can trigger Nrf2-dependent transcriptional activity in a K-loop-dependent manner.

mVP24 expression also induced expression of the endogenous ARE genes, NAD(P)H quinone oxidoreductase 1 (*NQO1*) and glutamate-cysteine ligase, modifier subunit (*GCLM*) (Lau et al., 2010), as assessed by quantitative RT-PCR (qRT-PCR) (Figures 3D and S3B). Neither the mVP24 mutants nor eVP24 induced expression of these genes (Figure S3). In contrast, eVP24 DIEPCCGE and eVP24 K-loop did induce significant levels of *GCLM* mRNA (Figures 3D and S3B). Correspondingly, NQO1 protein levels increased in the presence of wild-type but not mutated mVP24s, eVP24, or the eVP24 chimeras (Figures 3E and S3C). Interestingly, the eVP24 chimeras did not induce *NQO1* and induced *GCLM* mRNA to a lesser extent than did mVP24. This may reflect in part an as yet uncharacterized inhibitory activity of eVP24 on Nrf2-induced transcription responses that can be seen in ARE reporter gene assays (Figure S3D). Consistent with the ARE induction, cells transfected with Nrf2 (a positive control) or mVP24 were protected from killing by menadione, a compound that induces oxidative damage. In contrast, significant cell death was detected in the pCAGGS and mVP24 G211A/E212A-transfected cells (Figure 3F).

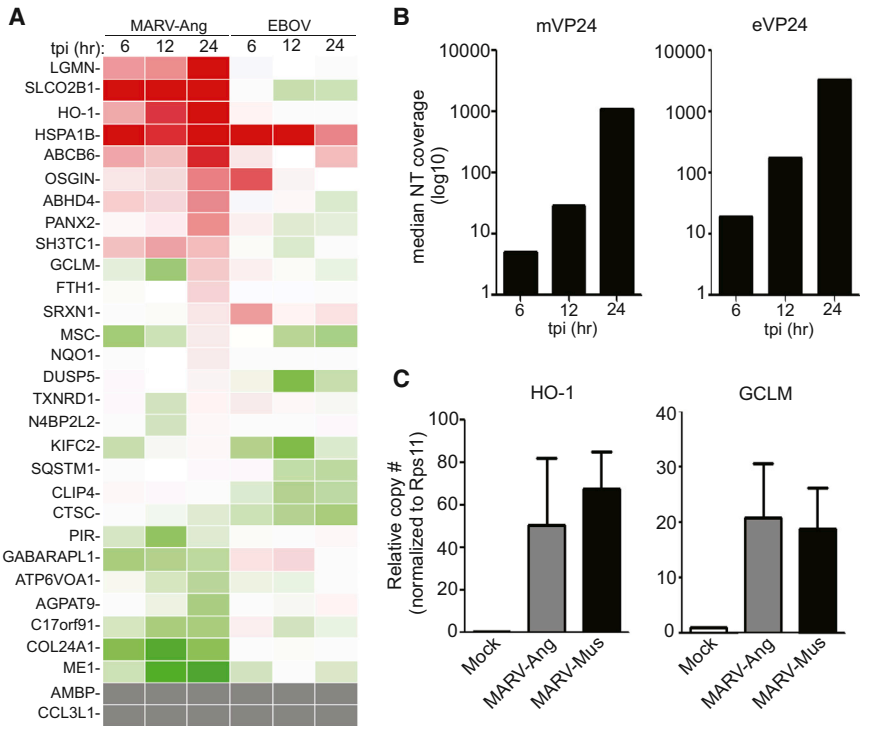

Figure 4. MARV Infection Upregulates the Nrf2 Antioxidant Pathway

(A and B) THP-1 cells were infected with MARV-Ang or Zaire EBOV (moi = 3) and subjected to expression analysis by mRNA sequencing (mRNA-seq).

(A) Heatmap displaying the expression profile of 30 Nrf2-activated genes (Chorley et al., 2012). Red indicates upregulated genes (maximum induction, 8.55-fold relative to mock-infected cells). Green indicates downregulated genes (lowest value, 0.2-fold relative to mock-infected cells). Gray indicates genes undetected in the mRNA-seq.

(B) mVP24 and eVP24 mRNA expression levels represented as median nucleotide coverage.

(C) THP-1 cells were infected with MARV-Ang or MARV-Mus (moi, 1) and subjected to qRT-PCR. Values were normalized to *RPS11*. Mock sample contains a single replicate; MARV-Ang and MARV-Mus represent the mean and SEM of triplicate samples.

See also Figure S4.

MARV Infection Induces the Expression of Nrf2-Responsive Genes

mVP24 activates Nrf2 via interaction with Keap1, but eVP24 does not, suggesting that MARV but not EBOV infection should induce an ARE response. To test this hypothesis, we profiled the expression of select ARE genes in THP-1 cells following MARV Angola strain (MARV-Ang) or Zaire EBOV infection (multiplicity of infection [moi], 3). A substantial number of ARE genes were upregulated in MARV-infected THP-1 cells as the infection progressed and mVP24 mRNA levels increased (Figures 4A and 4B). Although a few ARE genes were upregulated by EBOV infection, the response was not as global as was seen with MARV, and the response did not correlate well with eVP24 expression (Figures 4A and 4B). The mVP24 K-loop sequence is conserved among MARV strains, suggesting that ARE activation should also be shared between MARV strains. Indeed, induction of two representative ARE genes, heme oxygenase 1 (*HO-1*) and *GCLM*, was demonstrated by qRT-PCR following infection of THP-1 cells with MARV-Ang or Musoke (MARV-Mus) (Figure 4C). Interestingly, HO-1 is highly upregulated during MARV infection (Figure 4A), and a recent study has indicated that EBOV replication/transcription is inhibited by HO-1 expression (Hill-Batorski et al., 2013). However, using a MARV minigenome assay, we did not detect any inhibition following HO-1 overexpression (Figure S4; see Supplemental Results for further details), suggesting that upregulation of this ARE may not impair MARV replication.

DISCUSSION

The host antioxidant response has been increasingly recognized as relevant to virus infections. Here, we demonstrate a direct, high-affinity interaction between mVP24 and the Kelch domain of the human and bat Keap1, a major negative regulator of antioxidant responses (see also Supplemental Discussion on bat Keap1). This interaction, for which we define a critical role for the mVP24 K-loop sequence, can disrupt Nrf2-Keap1 interaction and induce a cytoprotective state through transcriptional activation of the ARE promoter. Although other viruses have previously been demonstrated to activate antioxidant responses, the mechanisms of activation appear indirect, with virus infection triggering oxidative stress or other cellular signaling pathways that stimulate Nrf2 nuclear accumulation (Burdette et al., 2010; Cho et al., 2009; Ivanov et al., 2011; Kesic et al., 2011; Lee et al., 2013; Schaedler et al., 2010). In contrast, the direct interaction between mVP24 and Keap1 provides compelling evidence that viruses have evolved mechanisms to engage the cellular antioxidant response as part of their replication strategy.

Keap1-Nrf2 interaction is required for negative regulation of the antioxidant response. A number of stimuli, such as oxidative stress, that perturb the Keap1-Nrf2 interaction stabilize Nrf2, allowing it to accumulate in the nucleus where it binds AREs and cooperates with other factors to activate ARE-containing promoters (Dinkova-Kostova et al., 2002; Zhang and Hannink, 2003). In addition, the interaction of the Keap1 Kelch domain with p62, an autophagy factor that functions in the clearance of polyubiquitinated complexes, activates Nrf2 through the disruption of binding via the lower-affinity Keap1 binding site on Nrf2 (Komatsu et al., 2010; Lau et al., 2010). We demonstrated that the mVP24-Keap1 interaction requires the Keap1 Kelch domain, as is true for many other Keap1 interactors (Kim et al., 2010; Komatsu et al., 2010; Lo and Hannink, 2006; Niture and Jaiswal, 2011). Our data further suggest that the interaction of mVP24 with Keap1 can disrupt the high-affinity Nrf2-Keap1 binding site, leading to the subsequent nuclear localization of Nrf2 and activation of the antioxidant response.

The structural basis for the Keap1 Kelch interaction with peptides derived from several cellular Keap1 binding partners, including Nrf2, p62, and prothymosin α, was previously described by Komatsu et al. (2010), Lo et al. (2006), and Padmanabhan et al. (2008). These peptides bind the bottom of the Keap1 β sheet propeller, which forms a basic pocket, in part through electrostatic interactions with Keap1 arginine residues. Common features of the binding peptides include acidic residues along with a GE motif (Komatsu et al., 2010; Lo and Hannink, 2006). Data obtained with mutated mVP24 K-loop acidic residues and the GE motif support a similar mode of binding for mVP24, although we cannot exclude a contribution of other parts of mVP24. Consistent with a model where the mVP24 loop and the acidic residues within the loop make analogous contacts with the Keap1 Kelch domain, substitution of Keap1 R415 to alanine abrogated Keap1-mVP24 interaction.

It is striking that MARVs and EBOVs differ in their interaction with the ARE response (see Supplemental Discussion for details). Although there are no structures of mVP24, several structures of eVP24s, including Sudan and Reston EBOVs (sVP24 and rVP24) (Zhang et al., 2012) as well as Zaire EBOV (eVP24), are available (Figure 2; PDB 4M0Q). In order to evaluate the mVP24 structure, we used the eVP24 structure, which was most complete as the basis for the Phyre2-threading model of mVP24. In the mVP24 model, the K-loop contains the DIEPCCGE sequence, a sequence that is not conserved between mVP24 and eVP24 but shows similarity to motifs of other Keap1-interacting "GE motifs." Replacement of the K-loop residues with a heterologous linker sequence or mutation to alanine of the D205 and E207 or of G211 and E212 was sufficient to greatly reduce or abrogate binding, although it should be acknowledged that the nuclear localization confounds interpretation of the G211A/E212A mutant data. That the DIEPCCGE loop is central to binding is confirmed by the fact that transfer of the loop to eVP24, which otherwise does not interact with Keap1, confers binding activity. Furthermore, wild-type mVP24 effectively competes with Nrf2 for binding to Keap1 in vitro and dissociates GFP-Nrf2 from Flag-Keap1 in a K-loop-dependent manner. These observations suggest a mechanism by which mVP24 activates an ARE transcriptional response. Interestingly, the mVP24 DIEPCCGE sequence diverges from other Keap1 binding motifs, such as the so-called ETGE motif of Nrf2 (DEETGE), with "PCC" inserted between "GE" and more amino-terminal acidic residues. The presence of the Cys residues is intriguing given that Keap1-Nrf2 interactions are regulated by oxidation. Whether these residues, which are not present in other Keap1-interacting motifs, play an important role in the mVP24-Keap1 interaction will be the subject of future studies.

In addition to the ARE response, Keap1 regulates other stress-induced cell survival pathways through interaction of its Kelch domain with a variety of proteins, including PGAM5, IKKβ, and p62 (Kim et al., 2010; Komatsu et al., 2010; Lau et al., 2010; Lee et al., 2009; Lo and Hannink, 2006; Niture and Jaiswal, 2011). mVP24 disruption of these Keap1 interactions could inhibit apoptosis, activate NF-κB-mediated cell survival pathways, and influence autophagy (Fan et al., 2010; Kim et al., 2010; Lee et al., 2009; Niture and Jaiswal, 2011). Furthermore, the stable interaction of mVP24 and Keap1, which did not detectably influence mVP24 expression levels, might allow the recruitment of Keap1 and binding partners for new functions. Further study is therefore required to fully elucidate the impact of the mVP24-Keap1 interaction upon MARV infection.

EXPERIMENTAL PROCEDURES

CoIP

Twenty-four hours posttransfection with the indicated plasmids, HEK293T cells were lysed in NP-40 lysis buffer (50 mM Tris [pH 7.5], 280 mM NaCl, 0.5% Nonidet P-40, 0.2 mM EDTA, 2 mM EGTA, 10% glycerol, and protease inhibitor [cOmplete; Roche]). Anti-FLAG M2 magnetic beads or anti-HA beads (Sigma-Aldrich) were incubated with lysates for 1 hr at 4°C, washed five times in NP-40 lysis buffer, and eluted using either 3× FLAG peptide (Sigma-Aldrich) or by boiling in sample loading buffer.

Activation of Nrf2

For ARE reporter gene assays, a commercially available reporter gene, pGL4.37[luc2P/ARE/Hygro] (ARE) (Promega), was cotransfected with a constitutively expressed *Renilla* luciferase reporter plasmid (pRL-tk; Promega), and the indicated protein expression plasmids. At 18 hr posttransfection, a dual luciferase reporter assay (Promega) was performed in triplicate, and firefly luciferase values were normalized to *Renilla* luciferase values. Statistical significance was assessed with one-way ANOVA using Tukey's test for comparisons to the control. Protein expression levels were assessed by western blot. Levels of endogenous *NQO1*, *GCLM*, or *HO-1* mRNAs were assessed by qRT-PCR, and NQO1 protein levels were assessed by western blot using a commercially available antibody (Santa Cruz Biotechnology).

Virus Infections

The following infections were performed under BSL-4 conditions at the Galveston National Laboratory. THP-1 cells were differentiated overnight with 100 nM PMA and infected with MARV-Ang (moi = 3 or 1), MARV-Mus (moi = 1), or EBOV (moi = 3). Viral total RNA was extracted with TRIzol at the indicated time points for analysis by deep sequencing or qRT-PCR. For deep sequencing, mRNA was purified with Oligo(dT) magnetic beads (Invitrogen). cDNA libraries were generated (NEBNext; New England Biolabs) and sequenced on the Illumina HiSeq 2500 platform, and relative expression for each gene of interest was determined. For qRT-PCR, cDNA was generated with Oligo(dT) primers, and relative expression for each gene of interest was determined by normalizing to the indicated housekeeping gene. Refer to Supplemental Experimental Procedures for additional details.

SUPPLEMENTAL INFORMATION

Supplemental Information includes Supplemental Results, Supplemental Discussion, Supplemental Experimental Procedures, four figures, and one table and can be found with this article online at http://dx.doi.org/10.1016/j.celrep.2014.01.043.

ACKNOWLEDGMENTS

This work was supported by NIH grants AI059536 (to C.F.B.) and AI081914 (to G.K.A.), DTRA grant HDTRA1-12-1-0051 (to C.F.B. and G.K.A.), and NSF graduate fellowship DGE-1143954 (to B.J.). All microscopy studies were performed with the generous assistance of the Icahn School of Medicine at Mount Sinai Microscopy Shared Resource Facility. Sequencing was performed at the Genomics Sequencing Facility at Mount Sinai. We thank Hardik Shah and the Bioinformatics Group of the Icahn Institute for Genomics and MultiScale Biology for help with sequence analysis. We thank Drs. S. Ginell, N. Duke, and J. Lazarz at the Structural Biology Center (Advanced Photon Source) and Dr. J. Nix at Beamline 4.2.2 (Advanced Light Source) for data collection support. Use of Argonne National Laboratory SBC beamlines at APS was supported by the U.S. D.O.E. contract DE-AC02-06CH11357.

Cell PRESS
Open ACCESS

Received: August 2, 2013
Revised: December 12, 2013
Accepted: January 30, 2014
Published: March 13, 2014

REFERENCES

Amman, B.R., Carroll, S.A., Reed, Z.D., Sealy, T.K., Balinandi, S., Swanepoel, R., Kemp, A., Erickson, B.R., Comer, J.A., Campbell, S., et al. (2012). Seasonal pulses of Marburg virus circulation in juvenile *Rousettus aegyptiacus* bats coincide with periods of increased risk of human infection. PLoS Pathog. *8*, e1002877.

Baird, L., and Dinkova-Kostova, A.T. (2011). The cytoprotective role of the Keap1-Nrf2 pathway. Arch. Toxicol. *85*, 241–272.

Bamberg, S., Kolesnikova, L., Möller, P., Klenk, H.D., and Becker, S. (2005). VP24 of Marburg virus influences formation of infectious particles. J. Virol. *79*, 13421–13433.

Beniac, D.R., Melito, P.L., Devarennes, S.L., Hiebert, S.L., Rabb, M.J., Lamboo, L.L., Jones, S.M., and Booth, T.F. (2012). The organisation of Ebola virus reveals a capacity for extensive, modular polyploidy. PLoS One *7*, e29608.

Bharat, T.A., Riches, J.D., Kolesnikova, L., Welsch, S., Krähling, V., Davey, N., Parsy, M.L., Becker, S., and Briggs, J.A. (2011). Cryo-electron tomography of Marburg virus particles and their morphogenesis within infected cells. PLoS Biol. *9*, e1001196.

Bharat, T.A., Noda, T., Riches, J.D., Kraehling, V., Kolesnikova, L., Becker, S., Kawaoka, Y., and Briggs, J.A. (2012). Structural dissection of Ebola virus and its assembly determinants using cryo-electron tomography. Proc. Natl. Acad. Sci. USA *109*, 4275–4280.

Brauburger, K., Hume, A.J., Mühlberger, E., and Olejnik, J. (2012). Forty-five years of Marburg virus research. Viruses *4*, 1878–1927.

Burdette, D., Olivarez, M., and Waris, G. (2010). Activation of transcription factor Nrf2 by hepatitis C virus induces the cell-survival pathway. J. Gen. Virol. *91*, 681–690.

Cho, H.Y., Imani, F., Miller-DeGraff, L., Walters, D., Melendi, G.A., Yamamoto, M., Polack, F.P., and Kleeberger, S.R. (2009). Antiviral activity of Nrf2 in a murine model of respiratory syncytial virus disease. Am. J. Respir. Crit. Care Med. *179*, 138–150.

Chorley, B.N., Campbell, M.R., Wang, X., Karaca, M., Sambandan, D., Bangura, F., Xue, P., Pi, J., Kleeberger, S.R., and Bell, D.A. (2012). Identification of novel NRF2-regulated genes by ChIP-Seq: influence on retinoid X receptor alpha. Nucleic Acids Res. *40*, 7416–7429.

Copple, I.M. (2012). The Keap1-Nrf2 cell defense pathway—a promising therapeutic target? Adv. Pharmacol. *63*, 43–79.

Dinkova-Kostova, A.T., Holtzclaw, W.D., Cole, R.N., Itoh, K., Wakabayashi, N., Katoh, Y., Yamamoto, M., and Talalay, P. (2002). Direct evidence that sulfhydryl groups of Keap1 are the sensors regulating induction of phase 2 enzymes that protect against carcinogens and oxidants. Proc. Natl. Acad. Sci. USA *99*, 11908–11913.

Fan, W., Tang, Z., Chen, D., Moughon, D., Ding, X., Chen, S., Zhu, M., and Zhong, Q. (2010). Keap1 facilitates p62-mediated ubiquitin aggregate clearance via autophagy. Autophagy *6*, 614–621.

Hill-Batorski, L., Halfmann, P., Neumann, G., and Kawaoka, Y. (2013). The cytoprotective enzyme heme oxygenase-1 suppresses Ebola virus replication. J. Virol. *87*, 13795–13802.

Hoenen, T., Groseth, A., Kolesnikova, L., Theriault, S., Ebihara, H., Hartlieb, B., Bamberg, S., Feldmann, H., Ströher, U., and Becker, S. (2006). Infection of naive target cells with virus-like particles: implications for the function of ebola virus VP24. J. Virol. *80*, 7260–7264.

Huang, Y., Xu, L., Sun, Y., and Nabel, G.J. (2002). The assembly of Ebola virus nucleocapsid requires virion-associated proteins 35 and 24 and posttranslational modification of nucleoprotein. Mol. Cell *10*, 307–316.

Itoh, K., Wakabayashi, N., Katoh, Y., Ishii, T., Igarashi, K., Engel, J.D., and Yamamoto, M. (1999). Keap1 represses nuclear activation of antioxidant responsive elements by Nrf2 through binding to the amino-terminal Neh2 domain. Genes Dev. *13*, 76–86.

Ivanov, A.V., Smirnova, O.A., Ivanova, O.N., Masalova, O.V., Kochetkov, S.N., and Isaguliants, M.G. (2011). Hepatitis C virus proteins activate NRF2/ARE pathway by distinct ROS-dependent and independent mechanisms in HUH7 cells. PLoS One *6*, e24957.

Kelley, L.A., and Sternberg, M.J. (2009). Protein structure prediction on the Web: a case study using the Phyre server. Nat. Protoc. *4*, 363–371.

Kesic, M.J., Simmons, S.O., Bauer, R., and Jaspers, I. (2011). Nrf2 expression modifies influenza A entry and replication in nasal epithelial cells. Free Radic. Biol. Med. *51*, 444–453.

Kim, J.E., You, D.J., Lee, C., Ahn, C., Seong, J.Y., and Hwang, J.I. (2010). Suppression of NF-kappaB signaling by KEAP1 regulation of IKKbeta activity through autophagic degradation and inhibition of phosphorylation. Cell. Signal. *22*, 1645–1654.

Komatsu, M., Kurokawa, H., Waguri, S., Taguchi, K., Kobayashi, A., Ichimura, Y., Sou, Y.S., Ueno, I., Sakamoto, A., Tong, K.I., et al. (2010). The selective autophagy substrate p62 activates the stress responsive transcription factor Nrf2 through inactivation of Keap1. Nat. Cell Biol. *12*, 213–223.

Lau, A., Wang, X.J., Zhao, F., Villeneuve, N.F., Wu, T., Jiang, T., Sun, Z., White, E., and Zhang, D.D. (2010). A noncanonical mechanism of Nrf2 activation by autophagy deficiency: direct interaction between Keap1 and p62. Mol. Cell. Biol. *30*, 3275–3285.

Lee, D.F., Kuo, H.P., Liu, M., Chou, C.K., Xia, W., Du, Y., Shen, J., Chen, C.T., Huo, L., Hsu, M.C., et al. (2009). KEAP1 E3 ligase-mediated downregulation of NF-kappaB signaling by targeting IKKbeta. Mol. Cell *36*, 131–140.

Lee, J., Koh, K., Kim, Y.E., Ahn, J.H., and Kim, S. (2013). Upregulation of Nrf2 expression by human cytomegalovirus infection protects host cells from oxidative stress. J. Gen. Virol. *94*, 1658–1668.

Lo, S.C., and Hannink, M. (2006). PGAM5, a Bcl-XL-interacting protein, is a novel substrate for the redox-regulated Keap1-dependent ubiquitin ligase complex. J. Biol. Chem. *281*, 37893–37903.

Lo, S.C., Li, X., Henzl, M.T., Beamer, L.J., and Hannink, M. (2006). Structure of the Keap1:Nrf2 interface provides mechanistic insight into Nrf2 signaling. EMBO J. *25*, 3605–3617.

Ma, Q. (2013). Role of nrf2 in oxidative stress and toxicity. Annu. Rev. Pharmacol. Toxicol. *53*, 401–426.

Magesh, S., Chen, Y., and Hu, L. (2012). Small molecule modulators of Keap1-Nrf2-ARE pathway as potential preventive and therapeutic agents. Med. Res. Rev. *32*, 687–726.

Mateo, M., Reid, S.P., Leung, L.W., Basler, C.F., and Volchkov, V.E. (2010). Ebolavirus VP24 binding to karyopherins is required for inhibition of interferon signaling. J. Virol. *84*, 1169–1175.

Mateo, M., Carbonnelle, C., Martinez, M.J., Reynard, O., Page, A., Volchkova, V.A., and Volchkov, V.E. (2011). Knockdown of Ebola virus VP24 impairs viral nucleocapsid assembly and prevents virus replication. J. Infect. Dis. *204* (*Suppl 3*), S892–S896.

McMahon, M., Itoh, K., Yamamoto, M., and Hayes, J.D. (2003). Keap1-dependent proteasomal degradation of transcription factor Nrf2 contributes to the negative regulation of antioxidant response element-driven gene expression. J. Biol. Chem. *278*, 21592–21600.

Niture, S.K., and Jaiswal, A.K. (2011). Inhibitor of Nrf2 (INrf2 or Keap1) protein degrades Bcl-xL via phosphoglycerate mutase 5 and controls cellular apoptosis. J. Biol. Chem. *286*, 44542–44556.

Noda, T., Ebihara, H., Muramoto, Y., Fujii, K., Takada, A., Sagara, H., Kim, J.H., Kida, H., Feldmann, H., and Kawaoka, Y. (2006). Assembly and budding of Ebolavirus. PLoS Pathog. *2*, e99.

Padmanabhan, B., Nakamura, Y., and Yokoyama, S. (2008). Structural analysis of the complex of Keap1 with a prothymosin alpha peptide. Acta Crystallogr. Sect. F Struct. Biol. Cryst. Commun. *64*, 233–238.

Pichlmair, A., Kandasamy, K., Alvisi, G., Mulhern, O., Sacco, R., Habjan, M., Binder, M., Stefanovic, A., Eberle, C.A., Goncalves, A., et al. (2012). Viral

immune modulators perturb the human molecular network by common and unique strategies. Nature *487*, 486–490.

Reid, S.P., Leung, L.W., Hartman, A.L., Martinez, O., Shaw, M.L., Carbonnelle, C., Volchkov, V.E., Nichol, S.T., and Basler, C.F. (2006). Ebola virus VP24 binds karyopherin alpha1 and blocks STAT1 nuclear accumulation. J. Virol. *80*, 5156–5167.

Reid, S.P., Valmas, C., Martinez, O., Sanchez, F.M., and Basler, C.F. (2007). Ebola virus VP24 proteins inhibit the interaction of NPI-1 subfamily karyopherin alpha proteins with activated STAT1. J. Virol. *81*, 13469–13477.

Schaedler, S., Krause, J., Himmelsbach, K., Carvajal-Yepes, M., Lieder, F., Klingel, K., Nassal, M., Weiss, T.S., Werner, S., and Hildt, E. (2010). Hepatitis B virus induces expression of antioxidant response element-regulated genes by activation of Nrf2. J. Biol. Chem. *285*, 41074–41086.

Tong, K.I., Katoh, Y., Kusunoki, H., Itoh, K., Tanaka, T., and Yamamoto, M. (2006). Keap1 recruits Neh2 through binding to ETGE and DLG motifs: characterization of the two-site molecular recognition model. Mol. Cell. Biol. *26*, 2887–2900.

Tong, K.I., Padmanabhan, B., Kobayashi, A., Shang, C., Hirotsu, Y., Yokoyama, S., and Yamamoto, M. (2007). Different electrostatic potentials define ETGE and DLG motifs as hinge and latch in oxidative stress response. Mol. Cell. Biol. *27*, 7511–7521.

Towner, J.S., Amman, B.R., Sealy, T.K., Carroll, S.A., Comer, J.A., Kemp, A., Swanepoel, R., Paddock, C.D., Balinandi, S., Khristova, M.L., et al. (2009). Isolation of genetically diverse Marburg viruses from Egyptian fruit bats. PLoS Pathog. *5*, e1000536.

Valmas, C., Grosch, M.N., Schümann, M., Olejnik, J., Martinez, O., Best, S.M., Krähling, V., Basler, C.F., and Mühlberger, E. (2010). Marburg virus evades interferon responses by a mechanism distinct from ebola virus. PLoS Pathog. *6*, e1000721.

Watanabe, S., Noda, T., Halfmann, P., Jasenosky, L., and Kawaoka, Y. (2007). Ebola virus (EBOV) VP24 inhibits transcription and replication of the EBOV genome. J. Infect. Dis. *196* (*Suppl 2*), S284–S290.

Wenigenrath, J., Kolesnikova, L., Hoenen, T., Mittler, E., and Becker, S. (2010). Establishment and application of an infectious virus-like particle system for Marburg virus. J. Gen. Virol. *91*, 1325–1334.

Zhang, D.D., and Hannink, M. (2003). Distinct cysteine residues in Keap1 are required for Keap1-dependent ubiquitination of Nrf2 and for stabilization of Nrf2 by chemopreventive agents and oxidative stress. Mol. Cell. Biol. *23*, 8137–8151.

Zhang, A.P., Bornholdt, Z.A., Liu, T., Abelson, D.M., Lee, D.E., Li, S., Woods, V.L., Jr., and Saphire, E.O. (2012). The ebola virus interferon antagonist VP24 directly binds STAT1 and has a novel, pyramidal fold. PLoS Pathog. *8*, e1002550.

Extended Results

Molecular modeling of mVP24 based on an eVP24 crystal structure. Filoviral VP24 proteins show significant sequence homology (data not shown). In order to gain insight into the structural basis for filoviral VP24 functions, we solved the crystal structure of the highly pathogenic Zaire EBOV VP24 protein (eVP24) (**Fig. S2, and Table S1** for structure statistics). Overall, the eVP24 structure adopts a conformation that is similar to those previously observed for the Reston virus and Sudan virus VP24 proteins (rVP24 and sVP24) (Zhang et al., 2012). In addition to the increased resolution to 1.92Å (compared to 2.0 Å and 2.1 Å rVP24 and sVP24 structures, respectively), many loop regions are experimentally well-defined in the eVP24 structure, particularly the residues that correspond to the mVP24 K-loop. For this reason, we chose to use the eVP24 structure for 1:1 threading using the mVP24 sequence. The resulting structure, shown in Fig. 1E, reveals that the critical K-loop of mVP24 is solvent exposed and is likely available to interact with the Keap1 Kelch domain. Previous studies of Keap1 Kelch interacting partners, such as Neh2 DLG, Neh2 ETGE, and p62, show that the peptide region binding to Kelch must be in an unfolded conformation (Cino et al., 2013). Consistent with these previous observations, our threaded model of mVP24 K-loop is predicted to be in a flexible conformation. While this data agrees with our binding studies and in vivo observations, additional structural data are required to experimentally confirm this observation.

mVP24 relocalizes Nrf2 to the nucleus. To determine whether interaction of mVP24 with the Keap1 Kelch domain activates Nrf2, a GFP-Nrf2 fusion protein was expressed alone or in the presence of Flag-Keap1 and HA-tagged wild-type mVP24, mutant mVP24 or wild-type or chimeric eVP24s. Over-expression of Nrf2, which overcomes endogenous Keap1, resulted in nuclear localization of GFP-Nrf2 (Fig. S1). Co-expression of Keap1 retained most of the Nrf2 in the cytoplasm. Additional expression of mVP24 restored Nrf2 nuclear localization in 72% of cells, suggesting disruption of the Nrf2-Keap1 interaction (**Fig. S1**). mVP24 linker, mVP24

D205A/E207A or mVP24 G211A/E212A did not prevent Keap1 retention of Nrf2 in the cytoplasm (Fig. S1). Expression of eVP24 also did not alter the cytoplasmic localization of Nrf2, but eVP24 K-loop resulted in 38% of cells having nuclear Nrf2 (**Fig. S1**). eVP24 DIEPCCGE, which precipitated less efficiently with Keap1 (**Fig. 1G**), was unable to relocalize Nrf2 to the nucleus (**Fig. S1**). Cumulatively, these data correlate mVP24-Keap1 interaction with the nuclear accumulation of Nrf2 and demonstrate that the presence of mVP24 can dissociate Nrf2 from Keap1.

Impact of HO-1 expression on a MARV minigenome assay. A recent study indicated that HO-1 expression inhibits EBOV replication/transcription (Hill-Batorski et al., 2013). As HO-1 is highly induced by MARV (**Fig. 4A**), we asked whether HO-1 expression affects MARV replication/transcription. When HO-1 was expressed in increasing amounts in the context of a MARV minigenome assay, no inhibitory effect was seen relative to a GFP over-expresion control (**Fig. S4**). These results suggest that HO-1 expression may not affect MARV replication/transcription in the manner recently described for EBOV.

Extended Discussion

We demonstrate that mVP24 interacts comparably with bat Keap1 and human Keap1 (**Fig. 1**). The conservation of the mVP24 interaction with bat Keap1 is consistent with a role for this interaction in MARV reservoir hosts. Although the Egyptian fruit bat (*Rousettus aegyptiacus*) is the most definitive host species for MARV, its Keap1 sequence was not available. We were able to obtain from public databases the predicted sequences of an Old World fruit bat (*Pteropus alecto*) and a New World insectivorous bat (*Myotis lucifugus*). Each of these was highly conserved across its entire length with human Keap1. Therefore, we presume that the Egyptian fruit bat Keap1 will also be highly conserved relative to human Keap1. Based on the *M. lucifugus* Keap1 sequence, we cloned Keap1 from an available *Myotis velifer incautus* cell line and demonstrated that the interaction with mVP24 is conserved. Further, because bat

Keap1 is very similar to human Keap1, we were able to test the functional implications of mVP24 for bat Keap1 in human cells, confirming that mVP24 can disrupt bat Keap1-(human) Nrf2 interaction. Pathogenesis of MARV in humans is almost certainly different than in the reservoir host. It is worth considering, therefore, that the mVP24-Keap1 interaction may have unique consequences in bats versus humans.

Oxidative stress responses upon MARV infection have not been characterized. We demonstrate that the expression of mVP24 as well as MARV infection can upregulate a number of Nrf2 targeted genes, whereas EBOV infection did not result in a comparable induction over time. Although the response of ARE genes to MARV versus EBOV infection is clearly different, not all of our chosen ARE genes were upregulated by MARV infection. Our list of ARE genes was based on 30 genes that were induced in lymphoid cells treated with the dietary isothiocyanate, sulforaphane (SFN) (Chorley et al., 2012). As some studies report that different activators of Nrf2 can upregulate different subsets of genes in the same cell type (Lau et al., 2013), it may not be surprising that all 30 genes did not increase. As would be expected for a functionally significant interaction, two different strains of MARV were able to upregulate an ARE response, as demonstrated by induction of two of the best characterized ARE genes, HO-1 and GCLM. Numerous effects of HO-1 expression have been described, including protection from apoptosis, modulation of the NFκB pathway and activation of the p38 mitogen-activated protein kinase (MAPK) pathway (reviewed in (Gozzelino et al., 2010)). GCLM is involved in the synthesis of glutathione, one of the major antioxidants in the cell (Ma, 2013). We hypothesize that upregulation of these, and other Nrf2 targeted genes, will enhance survival of MARV-infected cells, facilitating viral production.

Our data demonstrate that MARV and EBOV differ with regard to how they interact with the Nrf2 pathway. This is consistent with other functionally significant differences between these filoviral genera. Previously important differences have been described between MARV and

EBOV, including different mechanisms by which they inhibit innate immune responses. For example, eVP24 has been shown to interact with members of the NPI-1 subfamily of karyopherin alpha proteins to inhibit interferon signaling, but MARV VP24 does not (Mateo et al., 2009; Reid et al., 2006; Reid et al., 2007; Valmas et al., 2010). While MARV VP40 inhibits IFN signaling by blocking Jak1 function, EBOV VP40 does not (Valmas et al., 2010). Further, differences in the binding of MARV and EBOV VP35s to dsRNA suggest differences in how each virus antagonizes RIGI-like receptor signaling (Kimberlin et al., 2010; Leung et al., 2009; Leung et al., 2010a; Leung et al., 2010b; Ramanan et al., 2012b). Our data provides further evidence that there are significant differences between MARV and EBOV, despite the two viruses being in the same family.

Interestingly, HO-1 was recently reported to inhibit EBOV replication and inhibit an EBOV minigenome assay (Hill-Batorski et al., 2013). When we tested HO-1 expression for inhibitory activity towards a MARV minigenome assay, no suppressive activity was detected (Fig. S4). Inhibition of ARE responses by EBOV may suppress an anti-EBOV activity of HO-1. If MARV is resistant to the effects of HO-1, this may allow induction of HO-1 and other Nrf2-responsive genes for the purpose of enhancing cell survival.

The full implications of mVP24 interaction with Keap1 and a complete testing of the hypothesis that the interaction serves primarily to activate a cytoprotective state will require further study (see Discussion in main text). Nonetheless, some conclusions can be made. The induction of a cytoprotective state through the upregulation of ARE gene transcription would require the efficient translation of these cellular mRNAs. Because filoviruses do not shut down host cell transcription or protein synthesis, the ARE transcriptional response in MARV infected cells should lead to expression of cytoprotective proteins (Elliott et al., 1985; Hartman et al., 2008). Our hypothesis requires that infected cells survive long enough that virus yield can be enhanced. While little is known about MARV replication in the reservoir bat host, in many

human cell lines, the filovirus replication cycle is not particularly fast, and cells infected with EBOV have even been shown to undergo mitosis, demonstrating that these infections do not completely disrupt cellular processes (Hoenen et al., 2012). Therefore, the cytoprotective response would seem to have sufficient opportunity to be established during MARV infection. Also to be determined is whether other MARV proteins may modulate mVP24-Keap1 interaction.

It is notable that eVP24 seems to exert an inhibitory effect towards Nrf2-induced gene expression (**Fig. S3D**). The basis for this inhibition is unclear. This inhibitory activity may explain why the eVP24 chimeras containing mVP24 K-loop sequences do not activate ARE gene expression as well as wildtype mVP24 (**Fig. S3B and C**). Presumably, these eVP24 chimeras, which bind Keap1 efficiently, have two competing functions, an Nrf2 activating function (due to the interaction with Keap1) and an as yet unexplained inhibitory activity.

Filoviral VP24s also interact with filoviral VP35 and NP proteins in viral nucleocapsids, modulate viral RNA synthesis and play roles in viral budding (Bamberg et al., 2005; Beniac et al.; Bharat et al., 2012; Bharat et al., 2011; Hoenen et al., 2006; Huang et al., 2002; Mateo et al.; Noda et al., 2006; Watanabe et al., 2007; Wenigenrath et al., 2010). Further study will be required to understand the interplay and functional consequences of the various mVP24 interactions. A more complete understanding of these issues may suggest novel antiviral approaches to these deadly viruses.

Extended Experimental Procedures

Cells

HEK293T, HeLa and *Myotis velifer incautus* (ATCC, CRL-6012) cell lines were maintained in Dulbecco's minimal essential medium supplemented with 10% fetal bovine serum (FBS) and

cultured at 37°C and 5% CO_2. BSRT7 cells were grown in the same medium supplemented with 1% G418. THP-1 cells were maintained in RPMI supplemented with 10% FBS, 1% penicillin/streptomycin, 1% L-glutamine, 1% sodium pyruvate and 1% beta mercaptoethanol.

Plasmids

The plasmids encoding Flag and HA tagged mVP24 and eVP24 in the pCAGGS vector were previously described (Valmas et al., 2010). Mutations to mVP24 were made using overlapping PCR and cloned into pCAGGS vector containing a N-terminal Flag tag. Mutations of residues to alanines were done using the GCT codon. The serine/glycine linker, SGGSGGSG, in the mVP24 linker mutant was inserted into mVP24 using the forward primer 5'-TCCGGAGGCTCAGGTGGCAGCGGAacagtcctctcagaatcag-3' and the reverse primer 5'-TCCGCTGCCACCTGAGCCTCCGGAaatcctcctgacttccac-3' (the serine/glycine linker sequence is in capital letters). mVP24 residues 205-DIEPCCGE-212 were inserted into eVP24 between residues 202 and 211 using overlapping PCR, making eVP24 DIEPCCGE. mVP24 residues 202-RRIDIEPCCGETVLSESV-219 were inserted into eVP24 between residues 201 and 218 using overlapping PCR, making eVP24 K-loop. pcDNA Flag tagged Keap1 was purchased from Addgene (Addgene plasmid 28023(Fan et al., 2010)) and cloned with an N-terminal Flag tag into pCAGGS. A series of domain deletion mutants of Keap1 in Flag tagged pCAGGS were constructed by PCR. Keap1 ΔNTR construct lacks the first 60 amino acids, Keap1 ΔIVR lacks amino acids 180-314 and Keap1 ΔKelch/CTR lacks amino acids 315-624. Keap1 Kelch/CTR contains amino acids 315-624. Flag tagged Keap1 R415A was generated using overlapping PCR and the GCC codon to make the mutation to alanine. pcDNA3Myc tagged Nrf2 was purchased from Addgene (Addgene plasmid 21555(Furukawa and Xiong, 2005)) and cloned with an N-terminal HA tag or Flag tag into pCAGGS or into a pCAGGS GFP fusion construct. pcDNA4/TO HA p62 was purchased from Addgene (Addgene plasmid 28027). The pGL4.37[*luc2P*/ARE/Hygro] (ARE) reporter was purchased from Promega. HO-1 was cloned

using cDNA from THP-1 isolated RNA and the forward primer 5'-atggagcgtccgcaacccgac-3' and reverse primer 5'-tcacatggcataaagccctac-3' and inserted into pCAGGS such that it is expressed with an N-terminal HA tag. Bat-Keap1 and bat-Kelch were amplified from *Myotis velifer incautus* cell mRNA. For full length Keap1, forward primer 5'-atgcagccggaacccgggcc-3' and for the Kelch domain forward primer 5'-caggtgatgccctgccgg-3' were used. Each construct was amplified by using the same reverse primer 5'-tcaacaggtacagttctgctgg-3'. These amplicons were cloned into pCAGGS vector such that they produced a protein with an N-terminal Flag tag. MARV L was synthesized and cloned into pCAGGS such that it expressed with an N-terminal Flag tag. Flag-VP35 and Flag-NP have been previously described (Ramanan et al., 2012a).

Antibodies

Monoclonal mouse anti-FLAG M2 antibody, polyclonal rabbit anti-Flag antibody, monoclonal mouse anti-HA antibody and a polyclonal rabbit anti-HA antibody were purchased from Sigma-Aldrich. A mouse monoclonal anti-NQO1 (A180) antibody was purchased from Santa Cruz. Alexa Fluor anti-mouse 555 and Alexa Fluor anti-rabbit 633 were purchased from Invitrogen.

Isothermal Titration Calorimetry. All proteins were extensively dialyzed against buffer containing 10 mM HEPES (pH 7.0.), 150 mM sodium chloride, and 2 mM tris(2-carboxyethyl)phosphine and degassed before use. 110 μM Keap1 Kelch domain protein was loaded into a stirring syringe and injected into a sample cell containing 5 uM Nrf2 Neh2 domain protein or 7 μM mVP24 protein. Binding data were analyzed using Origin (OriginLab). The binding stoichiometry (n), enthalpy change (ΔH), entropy change (ΔS), and binding association constant (K_a) were obtained from the experimental titration curve. Dissociation constants (K_D) were calculated from the K_a.

Immunofluorescence

HeLa cells grown on glass coverslips were transfected with indicated plasmids using Lipofectamine 2000 (Invitrogen). At 24 hours post transfection, cells were fixed using 4%

paraformaldehyde and permeabilized using 0.1% Triton X-100. Cells were stained using the primary antibodies to Flag M2 (dilution 1:400) and HA (dilution 1:400) and secondary antibodies conjugated to Alexa Fluor 555 or Alexa Fluor 633 (Life Technologies) (dilution 1:2000). Images were taken using Zeiss Axioplan 2IE fluorescence microscope. The percent of cells containing nuclear Nrf2 localization was determined by counting cells in four individual fields of view.

Cell viability assay

HEK293T cells (10,000) were transfected using Lipofectamine 2000 (Invitrogen) with pCAGGS, Flag-Nrf2, mVP24 or mVP24 G211A/E212A plasmids. At 24 hours post transfection cells were treated with a vehicle control (ethanol) or 5uM of menadione (Sigma) for three hours, after which cells were assayed using CellTiter-Glo luminescent cell viability assay (Promega). The assay was performed with six replicates; error bars represent the SEM. Statistical analysis was done by one-way ANOVA using Tukey's test, *$p<0.05$.

Western Blotting

Lysates were run on 10% acrylamide SDS/PAGE gels (Lonza) and transferred to polyvinylidenedifluoride membrane. The membranes were probed with anti-FLAG M2, anti-HA and/or anti-NQO1 and developed using Western Lightning ECL kit (Perkin-Elmer).

RNA extractions and qRT-PCR

HEK293T cells (2.5×10^5) were transfected using Lipofectamine 2000 (Invitrogen) with the indicated plasmids. Cells were harvested at 24 hours post transfection. RNA was extracted using the RNeasy Kit (Qiagen), and cDNA was generated using SuperScript III Reverse Transcriptase (Invitrogen). Primers used for qRT-PCR were previously described (Lau et al., 2010). Transfections were performed in triplicate and the data were expressed as relative mRNA levels normalized to *RPS11*.

MARV minigenome assay

BSRT7 cells (2.5 x 10^5) were transfected in triplicate using Lipofectamine 2000 (Invitrogen) with the MARV minigenome plasmid (encoding *Renilla* luciferase) (200ng), a plasmid with firefly luciferase under the control of the T7 promoter as a transfection control (10ng), and plasmids encoding MARV L (500ng), MARV VP35 (125 ng) and MARV NP (500 ng). HA-HO-1 or GFP was co-transfected at increasing concentrations (100 ng, 500 ng and 1 μg). Forty-eight hours post-transfection a Dual luciferase assay (Promega) was performed. *Renilla* luciferase values were normalized to firefly luciferase values. Error bars represent the mean and SEM of triplicate samples, and statistical significance was assessed by a one-way ANOVA comparing bars as indicated using Tukey's test.

eVP24 cloning, expression, and purification

eVP24 was subcloned into a modified pET15b vector (Novagen) and sequenced before use. eVP24 was overexpressed as an MBP fusion protein in BL21(DE3) E. coli cells (Novagen) in LB medium. Protein expression was induced at an OD_{600nm} of 0.6 with 0.5 mM IPTG (Sigma) at 18°C. Cells were harvested, resuspended in buffer containing 25 mM sodium phosphate pH 7.5, 250 mM NaCl, 20 mM imidazole, and 5 mM 2-mecaptoethanol, and lysed using an EmulsiFlex-C5 homogenizer (Avestin). Cell lysate was clarified by centrifugation at 30,000 x *g* at 4 °C for 30 min. eVP24 protein was purified using a series of chromatographic columns. The MBP fusion tag was cleaved with TEV protease prior to loading on a Superdex 75 gel filtration column (GE Healthcare). Sample purity was determined by SDS-PAGE.

eVP24 crystallization, x-ray data collection, and structure determination

Initial crystallization conditions were obtained using commercially available screens (Hampton Research) and by the hanging drop method. Initial hits were further optimized using in-house reagents. Diffraction quality crystals were obtained in 150 mM MES pH 5.4, 20% Jeffamine M-600 pH 7.0, 50 mMCaCl, and 6 mMLiCl¬2 using 15 mg/ml of eVP24 protein. Crystals were cryo-protected with 25% glycerol prior to vitrification. X-ray diffraction data were collected at the

Advanced Light Source (ALS) beamline 4.2.2 (Berkeley, CA) initially and the final data were collected at the Advanced Photon Source (APS) beamline 19ID (Argonne, IL). The best eVP24 crystal diffracted to 1.92 Å. Diffraction data was processed using HKL3000 (Otwinowski and Minor, 1997). The structure was solved by molecular replacement with Molrep using PDB ID 3VNE and 4D9O as the search model and refined using REFMAC5 (Vagin et al, 2004). Manual model building was done in COOT (Emsley et al, 2004) with additional refinement using PHENIX1.8.2 (Adams, P.D, et al, 2010). The structure quality was assessed using MolProbity (Davis I. W et al, 2007).

In vitro pull-down assays.

Pull-down assays were performed in buffer containing 20 mMTris-HCl (pH 7.0), 50 mM sodium chloride, and 2 mM tris(2-carboxyethyl)phosphine. MBP-fusion mVP24 protein was immobilized on amylose resin prior to the addition of Keap1 Kelch domain and Nrf2 Neh2 domain. Bound resin was washed extensively. Samples were visualized by Coomassie blue staining of SDS-PAGE gels.

Supplemental References

Bamberg, S., Kolesnikova, L., Moller, P., Klenk, H.D., and Becker, S. (2005). VP24 of Marburg virus influences formation of infectious particles. J Virol *79*, 13421-13433.

Beniac, D.R., Melito, P.L., Devarennes, S.L., Hiebert, S.L., Rabb, M.J., Lamboo, L.L., Jones, S.M., and Booth, T.F. (2012). The organisation of Ebola virus reveals a capacity for extensive, modular polyploidy. PLoS One *7*, e29608.

Bharat, T.A., Noda, T., Riches, J.D., Kraehling, V., Kolesnikova, L., Becker, S., Kawaoka, Y., and Briggs, J.A. (2012). Structural dissection of Ebola virus and its assembly determinants using cryo-electron tomography. Proc Natl Acad Sci U S A *109*, 4275-4280.

Bharat, T.A., Riches, J.D., Kolesnikova, L., Welsch, S., Krahling, V., Davey, N., Parsy, M.L., Becker, S., and Briggs, J.A. (2011). Cryo-electron tomography of Marburg virus particles and their morphogenesis within infected cells. PLoS Biol *9*, e1001196.

Chorley, B.N., Campbell, M.R., Wang, X., Karaca, M., Sambandan, D., Bangura, F., Xue, P., Pi, J., Kleeberger, S.R., and Bell, D.A. (2012). Identification of novel NRF2-regulated genes by ChIP-Seq: influence on retinoid X receptor alpha. Nucleic Acids Res *40*, 7416-7429.

Cino, E.A., Killoran, R.C., Karttunen, M., and Choy, W.Y. (2013). Binding of disordered proteins to a protein hub. Sci Rep *3*, 2305.

Elliott, L.H., Kiley, M.P., and McCormick, J.B. (1985). Descriptive analysis of Ebola virus proteins. Virology *147*, 169-176.

Fan, W., Tang, Z., Chen, D., Moughon, D., Ding, X., Chen, S., Zhu, M., and Zhong, Q. (2010). Keap1 facilitates p62-mediated ubiquitin aggregate clearance via autophagy. Autophagy *6*, 614-621.

Furukawa, M., and Xiong, Y. (2005). BTB protein Keap1 targets antioxidant transcription factor Nrf2 for ubiquitination by the Cullin 3-Roc1 ligase. Molecular and cellular biology *25*, 162-171.

Gozzelino, R., Jeney, V., and Soares, M.P. (2010). Mechanisms of cell protection by heme oxygenase-1. Annu Rev Pharmacol Toxicol *50*, 323-354.

Hartman, A.L., Ling, L., Nichol, S.T., and Hibberd, M.L. (2008). Whole-genome expression profiling reveals that inhibition of host innate immune response pathways by Ebola virus can be reversed by a single amino acid change in the VP35 protein. J Virol *82*, 5348-5358.

Hill-Batorski, L., Halfmann, P., Neumann, G., and Kawaoka, Y. The Cytoprotective Enzyme Heme Oxygenase-1 Suppresses Ebola virus Replication. J Virol.

Hill-Batorski, L., Halfmann, P., Neumann, G., and Kawaoka, Y. (2013). The Cytoprotective Enzyme Heme Oxygenase-1 Suppresses Ebola Virus Replication. Journal of virology *87*, 13795-13802.

Hoenen, T., Groseth, A., Kolesnikova, L., Theriault, S., Ebihara, H., Hartlieb, B., Bamberg, S., Feldmann, H., Stroher, U., and Becker, S. (2006). Infection of naive target cells with virus-like particles: implications for the function of ebola virus VP24. J Virol *80*, 7260-7264.

Hoenen, T., Shabman, R.S., Groseth, A., Herwig, A., Weber, M., Schudt, G., Dolnik, O., Basler, C.F., Becker, S., and Feldmann, H. Inclusion bodies are a site of ebolavirus replication. J Virol *86*, 11779-11788.

Hoenen, T., Shabman, R.S., Groseth, A., Herwig, A., Weber, M., Schudt, G., Dolnik, O., Basler, C.F., Becker, S., and Feldmann, H. (2012). Inclusion bodies are a site of ebolavirus replication. Journal of virology *86*, 11779-11788.

Huang, Y., Xu, L., Sun, Y., and Nabel, G.J. (2002). The assembly of Ebola virus nucleocapsid requires virion-associated proteins 35 and 24 and posttranslational modification of nucleoprotein. Mol Cell *10*, 307-316.

Kimberlin, C.R., Bornholdt, Z.A., Li, S., Woods, V.L., Jr., MacRae, I.J., and Saphire, E.O. Ebolavirus VP35 uses a bimodal strategy to bind dsRNA for innate immune suppression. Proc Natl Acad Sci U S A *107*, 314-319.

Lau, A., Wang, X.J., Zhao, F., Villeneuve, N.F., Wu, T., Jiang, T., Sun, Z., White, E., and Zhang, D.D. (2010). A noncanonical mechanism of Nrf2 activation by autophagy deficiency: direct interaction between Keap1 and p62. Mol Cell Biol *30*, 3275-3285.

Lau, A., Zheng, Y., Tao, S., Wang, H., Whitman, S.A., White, E., and Zhang, D.D. (2013). Arsenic inhibits autophagic flux activating the Nrf2-Keap1 pathway in a p62-dependent manner. Mol Cell Biol.

Leung, D.W., Ginder, N.D., Fulton, D.B., Nix, J., Basler, C.F., Honzatko, R.B., and Amarasinghe, G.K. (2009). Structure of the Ebola VP35 interferon inhibitory domain. Proc Natl Acad Sci U S A *106*, 411-416.

Leung, D.W., Prins, K.C., Borek, D.M., Farahbakhsh, M., Tufariello, J.M., Ramanan, P., Nix, J.C., Helgeson, L.A., Otwinowski, Z., Honzatko, R.B.*, et al.* (2010a). Structural basis for dsRNA recognition and interferon antagonism by Ebola VP35. Nat Struct Mol Biol *17*, 165-172.

Leung, D.W., Shabman, R.S., Farahbakhsh, M., Prins, K.C., Borek, D.M., Wang, T., Muhlberger, E., Basler, C.F., and Amarasinghe, G.K. (2010b). Structural and functional characterization of Reston Ebola virus VP35 interferon inhibitory domain. J Mol Biol *399*, 347-357.

Ma, Q. (2013). Role of nrf2 in oxidative stress and toxicity. Annu Rev Pharmacol Toxicol *53*, 401-426.

Mateo, M., Carbonnelle, C., Martinez, M.J., Reynard, O., Page, A., Volchkova, V.A., and Volchkov, V.E. (2011). Knockdown of Ebola virus VP24 impairs viral nucleocapsid assembly and prevents virus replication. J Infect Dis *204 Suppl 3*, S892-896.

Mateo, M., Reid, S.P., Leung, L.W., Basler, C.F., and Volchkov, V.E. (2009). Ebolavirus VP24 binding to karyopherins is required for inhibition of interferon signaling. J Virol *84*, 1169-1175.

Noda, T., Ebihara, H., Muramoto, Y., Fujii, K., Takada, A., Sagara, H., Kim, J.H., Kida, H., Feldmann, H., and Kawaoka, Y. (2006). Assembly and budding of Ebolavirus. PLoS Pathog *2*, e99.

Otwinowski, Z., and Minor, W. (1997). Processing of X-ray diffraction data collected in oscilation mode. Methods Enzymol *276*, 307-326.

Ramanan, P., Edwards, M.R., Shabman, R.S., Leung, D.W., Endlich-Frazier, A.C., Borek, D.M., Otwinowski, Z., Liu, G., Huh, J., Basler, C.F.*, et al.* (2012a). Structural basis for Marburg virus VP35-mediated immune evasion mechanisms. Proceedings of the National Academy of Sciences of the United States of America *109*, 20661-20666.

Ramanan, P., Edwards, M.R., Shabman, R.S., Leung, D.W., Endlich-Frazier, A.C., Borek, D.M., Otwinowski, Z., Liu, G., Huh, J., Basler, C.F.*, et al.* (2012b). Structural basis for Marburg virus VP35-mediated immune evasion mechanisms. Proc Natl Acad Sci U S A *109*, 20661-20666.

Reid, S.P., Leung, L.W., Hartman, A.L., Martinez, O., Shaw, M.L., Carbonnelle, C., Volchkov, V.E., Nichol, S.T., and Basler, C.F. (2006). Ebola virus VP24 binds karyopherin alpha1 and blocks STAT1 nuclear accumulation. J Virol *80*, 5156-5167.

Reid, S.P., Valmas, C., Martinez, O., Sanchez, F.M., and Basler, C.F. (2007). Ebola virus VP24 proteins inhibit the interaction of NPI-1 subfamily karyopherin alpha proteins with activated STAT1. J Virol *81*, 13469-13477.

Valmas, C., Grosch, M.N., Schumann, M., Olejnik, J., Martinez, O., Best, S.M., Krahling, V., Basler, C.F., and Muhlberger, E. (2010). Marburg virus evades interferon responses by a mechanism distinct from ebola virus. PLoS Pathog *6*, e1000721.

Watanabe, S., Noda, T., Halfmann, P., Jasenosky, L., and Kawaoka, Y. (2007). Ebola virus (EBOV) VP24 inhibits transcription and replication of the EBOV genome. J Infect Dis *196 Suppl 2*, S284-290.

Wenigenrath, J., Kolesnikova, L., Hoenen, T., Mittler, E., and Becker, S. (2010). Establishment and application of an infectious virus-like particle system for Marburg virus. J Gen Virol *91*, 1325-1334.

Zhang, A.P., Bornholdt, Z.A., Liu, T., Abelson, D.M., Lee, D.E., Li, S., Woods, V.L., Jr., and Saphire, E.O. (2012). The ebola virus interferon antagonist VP24 directly binds STAT1 and has a novel, pyramidal fold. PLoS Pathog *8*, e1002550.

SUPPLEMENTAL TABLE

Table S1. Data collection, structure solution, and refinement statistics, related to Figure 2.

Data collection	
Space Group	$P4_32_12$
Unit cell parameters	
a, b, c (Å)	71.775, 71.775, 191.165
α, β, γ (°)	90, 90, 90
Resolution range (Å)	50 – 1.92
	(1.95 – 1.92)
Unique reflections	39161 (1923)
Redundancy	9.6 (9.7)
Completeness (%)	100.0(100.0)
R_{merge}(%)	8.9 (96.3)
$I / I\sigma$	33.2 (2.3)
Structure solution and refinement	
Resolution (Å)	33.60 – 1.92
	(1.97 – 1.92)
No. of reflections	39068
Completeness (%)	99.98 (99.90)
non-hydrogen atoms	3536
R_{work} / R_{free} (%)	20.21/22.93
	(24.88/28.62)
R.m.s. deviations	
Bond lengths (Å)	0.012
Bond angles (°)	1.575
B-factors (Å^2)	
Protein Chain A	44.75
Chain B	43.71
Water	45.29
Ramachandran plot outliers (%)	0.5
Molprobity score	2.02
Molprobity clash score	7.94

Experimental and refinement parameters were calculated as described in methods using standard methods. Values in parentheses are for the highest resolution shell 1.95 – 1.92 Å for data collection and for 1.97-1.92 Å for refinement.

Edwards et al. Figure S1

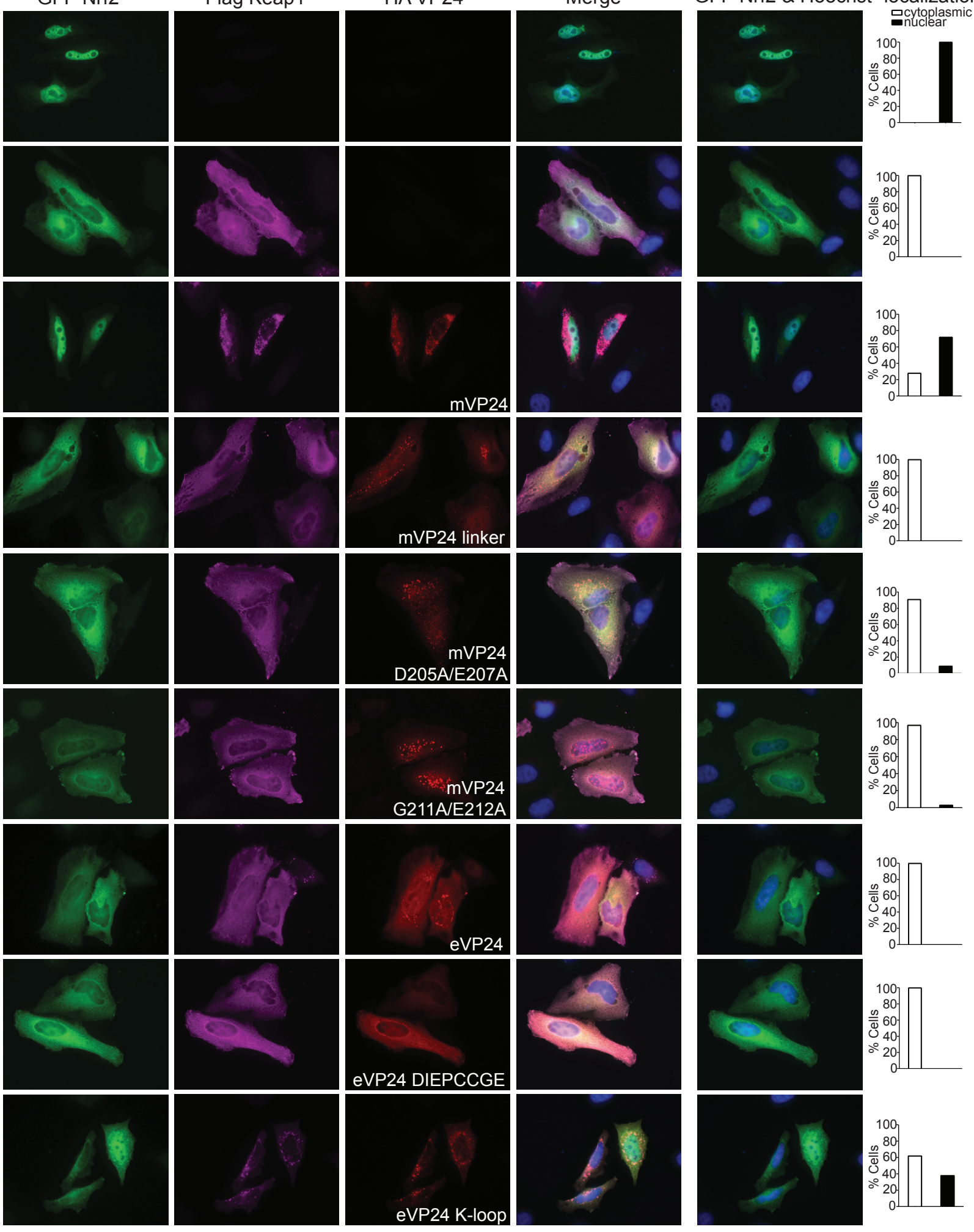

Fig. S1. mVP24 co-localizes with Keap1 and expression relocalizes Nrf2 to the nucleus, related to Figure 1. HeLa cells were transfected with plasmids for GFP-Nrf2, Flag-Keap1 and/or HA-tagged VP24 proteins. Twenty-four hours post transfection, slides were fixed and stained with anti-Flag antibody and anti-rabbit IgG Alexa Fluor 633 or anti-HA antibody and anti-mouse IgG Alexa Fluor 555 to visualize protein localization. Image is representative. The percent of cells with cytoplasmic vs. nuclear Nrf2 was determined by counting cells in four individual fields of view for each sample.

Edwards et al. Figure S2

A

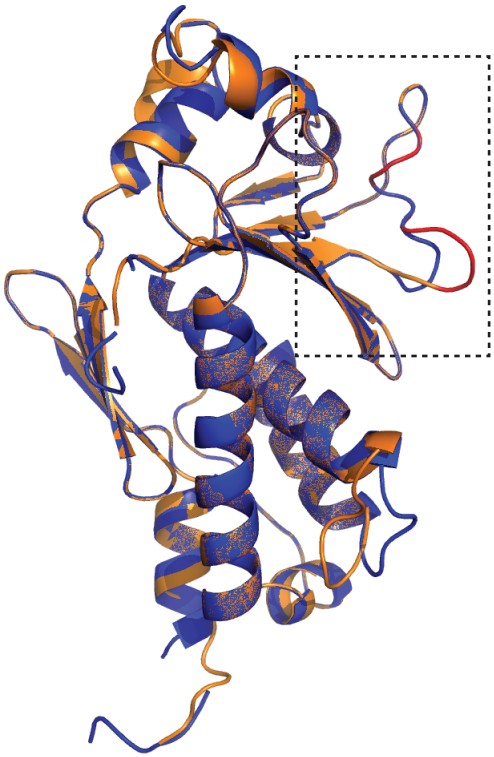

B

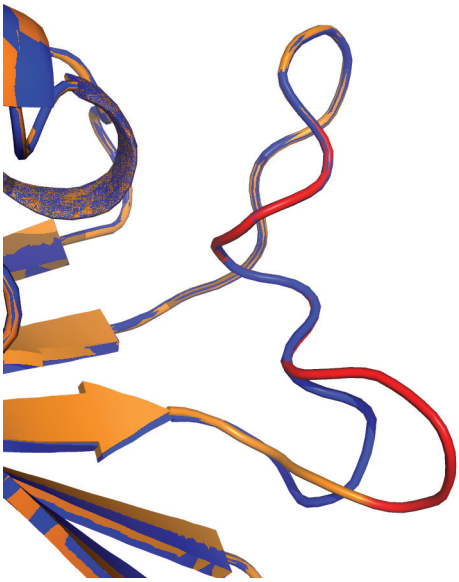

C

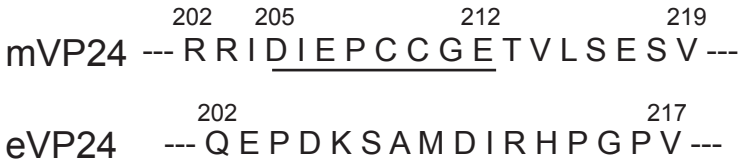

D

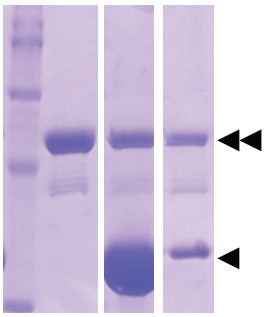

E

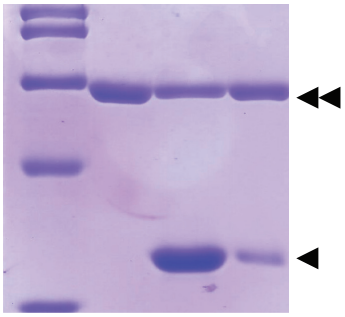

F

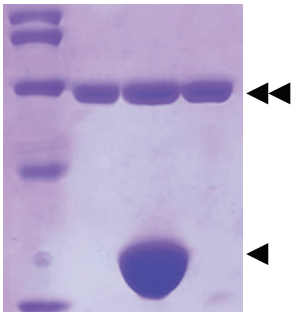

G

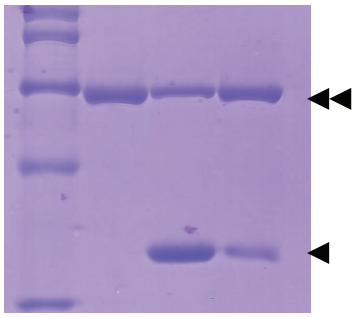

Fig. S2. mVP24 K-loop residues in the eVP24 scaffold are sufficient to mediate interactions between VP24 and the Keap1 Kelch domain, related to Figure 2. (A and B) Alignment of the Phyre2 generated structural model of mVP24 (orange) based on the eVP24 (purple) crystal structure (PDB ID 4M0Q). Residues in the K-loop are highlighted and expanded in (B). mVP24 K-loop residues 205-212 are highlighted in red. (C) Schematic representation of residues present in the loop regions of mVP24 and eVP24 highlighted in (B). (D, E, F and G) Coomassie blue-stained SDS-PAGE of pulldown assays of the Keap1 Kelch domain with: D. MBP-Nrf2 Neh2, E. MBP-mVP24, F. MBP-eVP24, and G. MBP-eVP24 K-loop. Lanes from left to right correspond to marker, amylose resin bound to MBP-tagged protein (double arrowheads), Keap1 Kelch domain (single arrowhead) added to amylose resin bound to MBP-tagged protein, and final bound amylose resin after washes.

Edwards et al. Figure S3

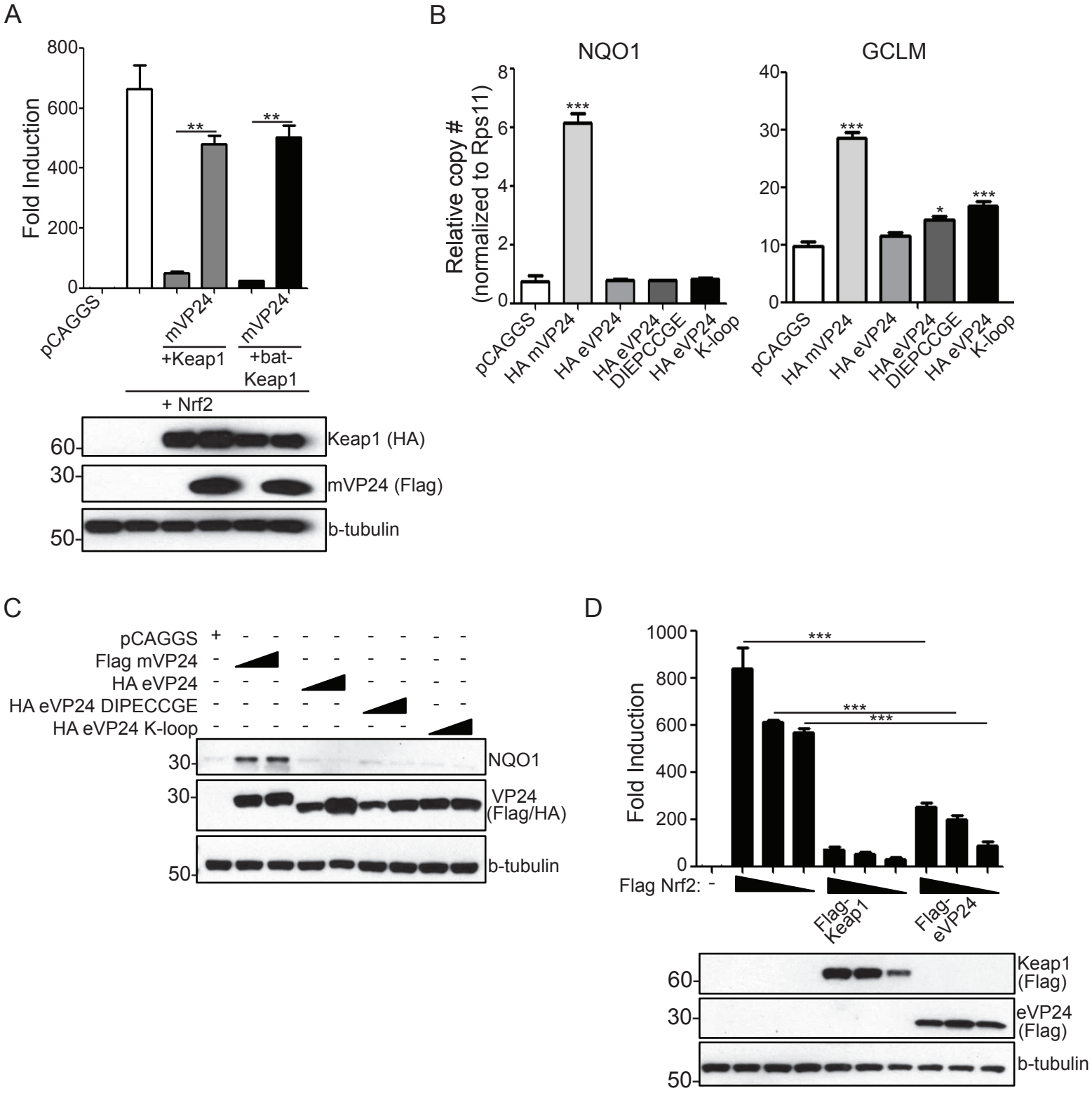

Fig. S3. Interaction of VP24 constructs with Keap1 activates ARE gene expression, related to Figure 3. 293T cells were transfected with the ARE luciferase reporter plasmid, a constitutively expressed *Renilla* luciferase plasmid, Flag-Nrf2, HA-Keap1 and pCAGGS (empty vector) or Keap1 or bat-Keap1 and Flag mVP24 as indicated. At 18 hpt luciferase activity was assayed. Western blots for HA and Flag are indicated. (B) pCAGGS, HA-mVP24, eVP24, eVP24 DIEPCCGE or eVP24 K-loop were transfected in triplicate in HEK293T cells. At 24 hpt, qRT-PCR was performed for the indicated mRNAs and normalized to *RPS11*. (C) 293T cells were transfected with the indicated plasmids, and 18 hpt endogenous NQO1 was measured by western blot. (D) The same assay protocol as in (A) but with Flag-Nrf2, Keap1 and eVP24 transfected as indicated. (A, B and D) represent the mean and SEM of triplicate samples, and statistical significance was assessed by a one-way ANOVA comparing columns to the control (white bar) or as indicated, ***$p<0.001$, **$p<0.01$ and *$p<0.05$.

Edwards et al. Figure S4

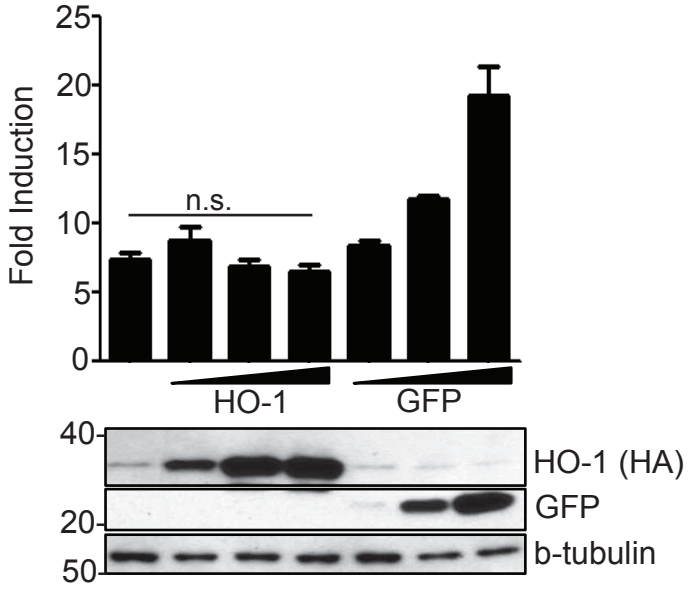

Fig. S4. MARV replication/transcription is not detectably affected by HO-1 expression, related to Figure 4. BSRT7 cells were transfected with the MARV *Renilla* luciferase minigenome, firefly luciferase as transfection control, and MARV L, VP35 and NP. HA-HO-1 or GFP were co-transfected at increasing concentrations (100ng, 500ng and 1ug). Forty-eight hpt luciferase activity was assayed. Bars represent the mean and SEM of triplicate samples and statistical significance was assessed by a one-way ANOVA comparing bars as indicated. n.s., no significance.